Geochemical evidence of drying during the 4.2 ka event in sediment cores from the Yucatán Peninsula, Mexico

Derek K. Gibson[1], Jonathan Obrist-Farner[2], Alex Correa-Metrio[3], Alejandra Rodriguez-Abaunza[4,5], Carlos Castañeda-Posadas[6]

[1.] School of Earth Systems and Sustainability, Southern Illinois University, Carbondale, IL, USA 62901

[2.] Department of Earth Sciences and Engineering, Missouri University of Science and Technology, Rolla, MO, USA 65409

[3.] Instituto de Geociencias, Universidad Nacional Autónoma de México, Querétaro, MX 76230

[4.] Department of Earth and Environmental Sciences, Indiana University Indianapolis, Indianapolis, IN, USA 46202

[5.] Posgrado en Ciencias del Mar y Limnología, Universidad Nacional Autónoma de México, Cd. de México, MX 04510

[6.] Laboratorio de Paleobiología, Herbario y Jardín Botánico Universitario, Ecocampus-Valsequillo, Benemérita Universidad Autónoma de Puebla, Puebla, MX 72960

Highlights

- Proxy data indicate dry conditions in lowland Mesoamerica during the 4.2 ka event
- Yucatán hydroclimate records indicate regionally coherent drying ca. 3.8 to 4.5 ka
- ENSO may have contributed to widespread drying during the end of the mid-Holocene

Abstract

Tropical hydroclimate variability during the Middle and Late Holocene was investigated using geochemical indicators of local-scale precipitation and evaporation preserved in sediment cores from two sites in the Mexican Yucatán Peninsula. Scanning X-Ray fluorescence spectroscopy data show generally decreasing precipitation trends during the Early and Middle Holocene. During the transition between the Middle and Late Holocene, geochemical evidence of reduced watershed erosion and increased evaporation indicate that a centennial-scale drying event impacted the region between 4.3 and 4.0 ka (kilo-anum; thousand years before present). These findings suggest that the 4.2 ka drying event, which has been previously recorded in Europe, Asia, and North and South America, also impacted the northern Neotropics. A comparison between our data and existing regional hydroclimate records suggests that dry conditions during the 4.2 ka event were coherent across western Central America. The timing of these regionally dry conditions coincided with a reduction in zonal sea surface temperature gradients in the tropical Pacific Ocean and a consequent mean-state increase in the frequency of El Niño events, suggesting that linkages between Pacific Ocean-atmosphere dynamics played a significant role in the regional drying that occurred during that time. These data provide new support for a Central American expression of the 4.2 ka event.

Key words

Holocene; Mesoamerica; Geochemistry; Paleoclimatology; Hydroclimate

1. Introduction

The transition from the middle to the Late Holocene was characterized by an anomalous drying event that has been identified in sediment (Booth et al., 2005; Arz et al., 2006; Nakamura et al., 2016), speleothem (Zhang et al., 2018), and ice core (Thompson et al., 2002) records. This event, known as the "4.2 ka event," has been recorded between 4.3 and 3.8 ka (kilo-anum; thousand years before present) around the world (Bini et al., 2019) and has been implicated in the societal collapse of many preindustrial societies, particularly across East Asia and the Levant (Liu and Feng, 2012; Meller et al., 2015). Because of the widespread evidence of this event in the geologic record, 4.2 ka was officially recognized as the stratigraphic marker between the Middle and Late Holocene (Toth and Aronson, 2019; Shankar, 2021). Despite numerous records of the 4.2 ka event from study sites across a broad range of geographic settings, the primary drivers of widespread drying during this interval are still widely debated (Walker et al., 2012; Toth and Aronson, 2019).

While previous work has linked mean-state hydroclimate changes during the 4.2 ka event to climatic variability associated with the El Niño-Southern Oscillation (ENSO) (Li et al., 2018; Marchant and Hooghiemstra, 2004), a full understanding of the synoptic origins and spatial extent of the 4.2 ka event have been hindered by a paucity of records from northern tropical America and the Southern Hemisphere (Railsback et al., 2018), with the former being of particular importance due to ENSO's influence on the hydroclimate of tropical America (Durán-Quesada et al., 2017). In particular, study sites that record this event in the Western Hemisphere have thus far been primarily confined to high latitude regions of Canada, the United States, and the southern Neotropics (Booth et al., 2005; Ohlendorf et al., 2014). To evaluate the global expression of the 4.2 ka event and better understand the potential ocean-atmosphere drivers of hydroclimate variability during that time, additional records from the northern Neotropics are necessary.

To address this need, we present an ~8,000-year record of hydroclimatic variability developed from sediment cores recovered from two sites in the Yucatán Peninsula of Mexico. Geochemical indicators of evaporation and environmental change in these watersheds are compared with other hydroclimate records that span the same interval to assess the consistency of regional hydrologic variability during the 4.2 ka event. Together, these datasets are synthesized with Holocene records of synoptic scale ocean-atmosphere processes to provide context regarding the possible driving mechanisms and spatial extent of global hydroclimate change during the middle and Late Holocene.

2. Study region

2.1 Modern climatology of the Yucatán Peninsula

Our study sites are located in the Mexican Yucatán Peninsula between 17˚ 48' to 21˚ 35' N and 86˚ 48' to 92˚ 27' W. Average near-surface air temperature in the region ranges between ~24˚ C during the winter and ~28˚ C during the late spring and early summer, with an annual average of ~26˚ C (Fig. 1, B and C; Pérez et al., 2011). The peninsula is characterized by a precipitation gradient from ~600 mm/yr in the northwest to ~2500 mm/yr in the southeast (de la Barreda et al., 2020). Across the region, most of the precipitation is in the form of summer and early autumn convective rainstorms, driven by the northerly migration of the Inter-tropical Convergence Zone (ITCZ) and intense heating and consequent easterly moisture flux from the

North Atlantic Warm Pool (Amador et al., 2006; Curtis, 2013; Sáenz et al., 2023). Notably, the Mexican Yucatán Peninsula does not experience a strong midsummer drought, unlike many other regions across Central America (Magaña et al., 1999). During winter, the southerly migration of the ITCZ and expansion of the Bermuda high pressure system decreases convection and increases atmospheric subsidence, resulting in decreased rainfall (de la Barreda et al., 2020).

Over multiannual to decadal timescales, precipitation across the Yucatán Peninsula is further modulated by combined ocean-atmosphere phenomena such as ENSO and the North Atlantic Oscillation (NAO) (Durán-Quesada et al., 2020; Obrist-Farner et al.,2023). In this region, positive ENSO cycles are characterized by reduced precipitation due to tropospheric warming generated by increased convection in the eastern tropical Pacific Ocean, which weakens the Atlantic component of the ITCZ (Giannini et al., 2001; Martinez et al., 2020). However, positive ENSO conditions increase tropical Atlantic sea-surface temperatures (SSTs), which increase moisture flux and consequent precipitation following an El Niño event. As a result, the initial phase of El Niño across the Yucatán Peninsula is anomalously dry, while the latter stages are comparatively wet (Giannini et al., 2001). Despite increased precipitation during the latter stages, the overall signal recorded across the Yucatán Peninsula during an El Niño event is that of reduced precipitation, due to the very dry conditions during the early phase of El Niño development (de la Barreda et al., 2020).

During the Late Holocene and through the present, precipitation responses in some regions of the Yucatán Peninsula are generally antiphased with the NAO signal, with +NAO conditions associated with reduced rainfall and vice versa (Bhattacharya et al., 2017; Gibson et al., 2024). Under +NAO conditions, the Caribbean Low-Level Jet is strengthened and driven to the south by an expanded North Atlantic Subtropical High pressure system, which cools tropical

Atlantic SSTs and reduces moisture flux from the Caribbean Sea to Central America (Wang, 2007; Anderson et al., 2019). NAO oscillations occur over daily to monthly time scales (Wanner et al., 2001); however, long-term shifts in the mean-state of the NAO also occur on multi-annual and decadal scales (Joyce et al., 2000).

2.2 Lake Yalahau

Lake Yalahau (20°39'25.25" N, 89°12'59.89" W; 2 m above sea level; Fig. 2) is located in the northwestern Yucatán Peninsula, in the Mexican state of Yucatán. It is the largest lake in the northern Yucatán Peninsula, with a surface area of 0.25 km^2. Watershed topography at Lake Yalahau is characterized by low relief and very little topographic variability, with elevations ranging from 2 to 50 m above sea level (Fig. 2 C). The lake is one of the many cenotes that exist across the northern Yucatán Peninsula, which were formed by sinkholes that developed in the karstic bedrock and subsequently filled with water as sea levels rose during the Early Holocene (Milliken et al., 2008; Rodriguez-Abaunza and Correa-Metrio, 2023). Typical of other cenotes in the region, the Lake Yalahau basin has steeply sloped littoral zones and a generally flat bottom. Water column depth was determined by depth measurements across the profundal zone, and ranged from 9 to 12 m. While there are no surface inlets or outflows from Lake Yalahau, lake level is maintained via a connection with the local water table, resulting in generally consistent lake volume and levels through time, regardless of changes in precipitation.

Lake Yalahau is located near the driest region of the Yucatán Peninsula, with the nearest meteorological station indicating a mean annual precipitation of 840 mm (data from 1986 to 2020, Servicio Meteorológico Nacional, 2024a; Fig 1A). The relatively low precipitation made

Lake Yalahau a valuable freshwater resource for local Maya communities, the populations of which reached significant sizes between ~4.8 to 1 ka (Dunning et al., 2013).

2.3 Laguna Maravillas

Laguna Maravillas (18°29'36.49" N, 90°16'25.55" W; 48 m above sea level; Fig. 2) is a small, shallow lake located in the southwestern Yucatán Peninsula in the Mexican state of Campeche. The littoral zone is less steep than at Lake Yalahau and contains abundant aquatic plants. Laguna Maravillas has a surface area of 9.2 km^2. Profundal depths were determined by depth measurements around the lake basin and ranged from 0.75 to 2.1 m. The lake is situated in an alluvial plain with generally low relief (surface elevation ranges from 40 to 200 m above sea level; Fig. 2 B), characterized by numerous small streams and floodplains. However, the Laguna Maravillas basin is not connected to any surficial inlets or outflows. As a result, the lake behaves as a hydrologically closed basin and experiences large amplitude year-to-year variability in lake level and volume, which are driven by the local balance of precipitation to evaporation. The carbonate bedrock and the warm, humid climate have led to the development of mature karst throughout the region, which has created an undulating landscape of karst depressions, many of which hold surface water in the form of lakes and wetlands (Marín-Stillman et al., 2004). According to the nearest meteorological station, mean annual precipitation at the site is 1210 mm/yr, ~70% of which is delivered during the summer rainy season (data from 1958 to 2020, Servicio Meteorológico Nacional, 2024b; Fig 1B). The vegetation surrounding the lake is composed mainly of medium and low semi-evergreen tropical forest. However, anthropogenic land use has disturbed much of the natural primary forests in the region (Torrescano-Valle and Islebe, 2015).

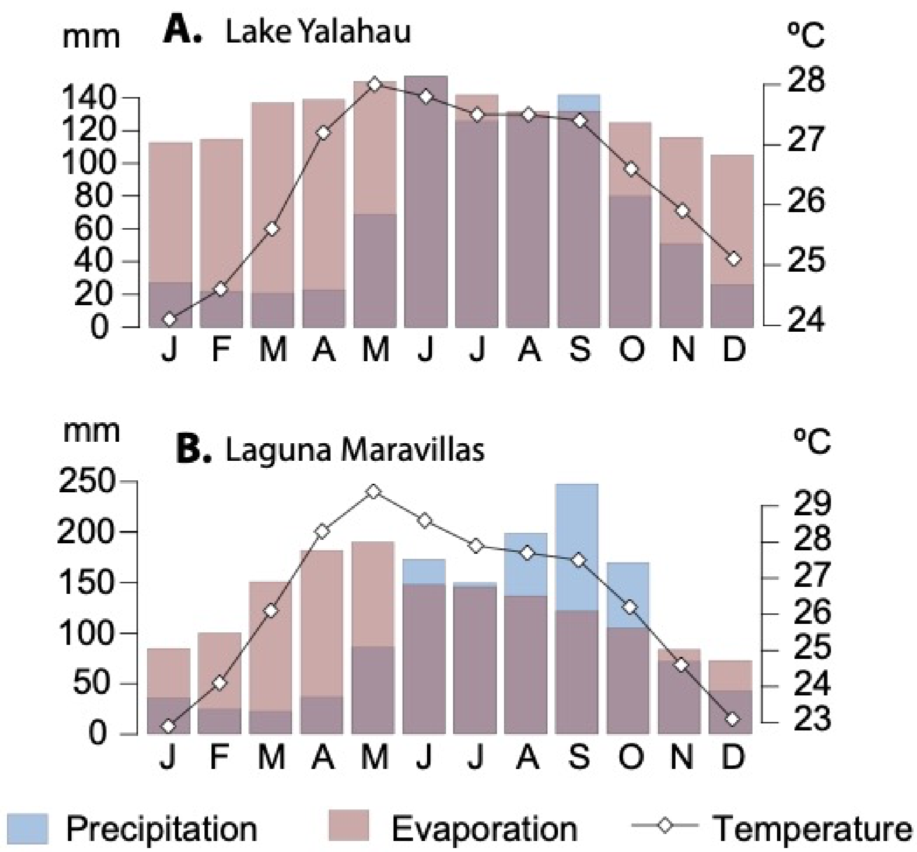

Fig. 1. Climographs showing average annual precipitation, evaporation, and temperature for **A.** Lake Yalahau and **B.** Laguna Maravillas (Servicio Meteorológico Nacional, 2024a; Servicio Meteorológico Nacional, 2024b).

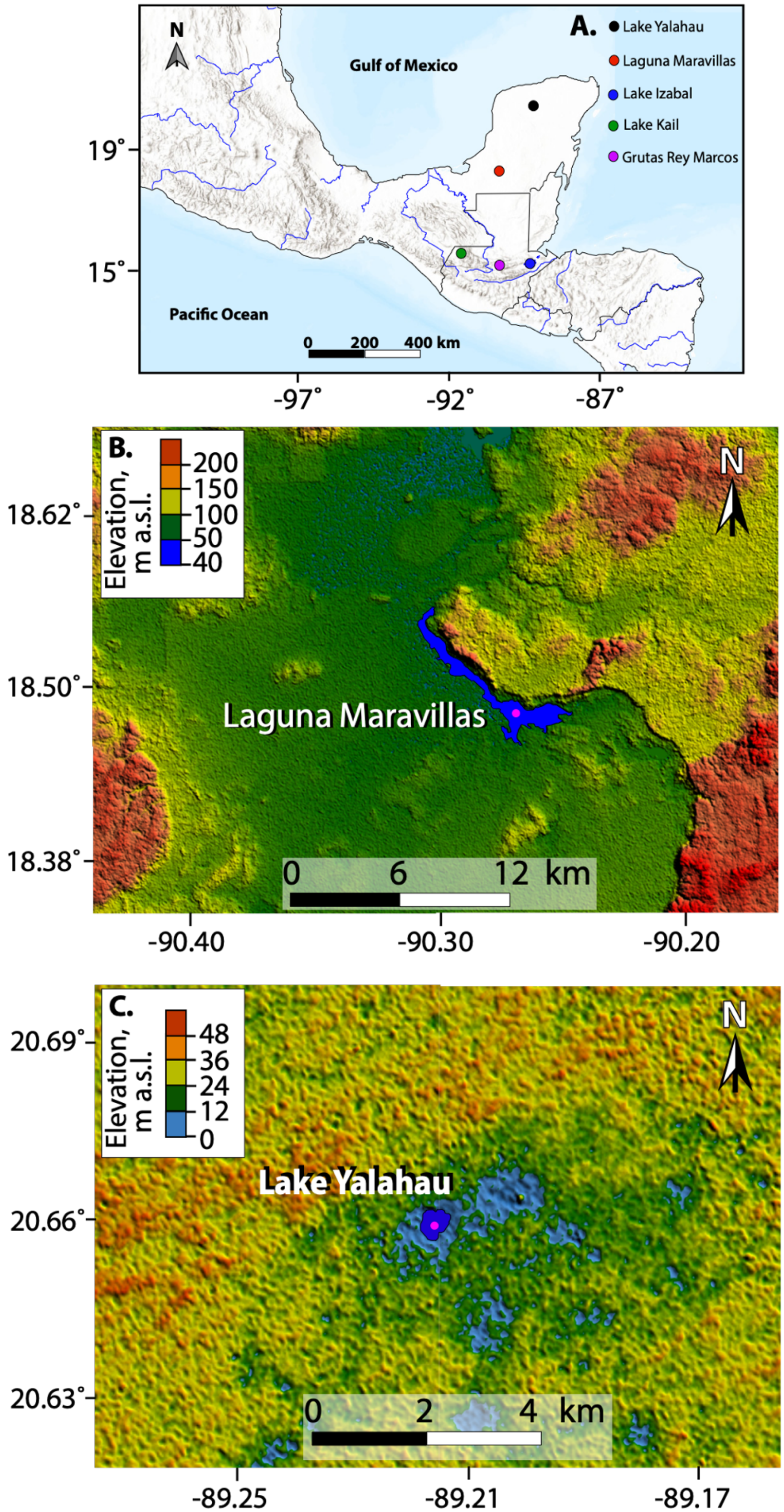
A.
Lake Yalahau
Laguna Maravillas
Lake Izabal
Lake Kail
Grutas Rey Marcos
N
Gulf of Mexico
Pacific Ocean
0 200 400 km
19°
15°
-97°
-92°
-87°
B.
Elevation, m a.s.l.
200
150
100
50
40
N
Laguna Maravillas
0 6 12 km
18.62°
18.50°
18.38°
-90.40
-90.30
-90.20
C.
Elevation, m a.s.l.
48
36
24
12
0
N
Lake Yalahau
0 2 4 km
20.69°
20.66°
20.63°
-89.25
-89.21
-89.17

Fig. 2. A. Regional map of the study area, showing the locations of Lake Yalahau and Laguna Maravillas and other paleoclimate records referenced herein. Panels **B.** and **C.** show the local topography surrounding Laguna Maravillas and Lake Yalahau, respectively. Sediment coring locations are marked by red dots.

3. Methods

3.1 Sediment core recovery

Sediment cores were recovered in from Laguna Maravillas in 2022 and Lake Yalahau in 2023 using a modified piston corer (Colinvaux et al., 1999), hand-pushed from a floating platform. In both lakes, two adjacent and overlapping cores were recovered from the deepest measured point to ensure complete core recovery. At Lake Yalahau, a separate piston corer, designed to capture the sediment-water interface was used to collect the uppermost, water-saturated sediments. These unconsolidated sediments were extruded vertically in the field, sectioned at 2.0-cm intervals, and transferred into labeled Whirl-Pak® bags, while the consolidated core sections from both sites were transported to Missouri University of Science and Technology and kept at ~4° C until analysis.

3.2 Age control

Age control for Laguna Maravillas was established via radiocarbon accelerator mass spectroscopy (AMS ^{14}C) of detrital charcoal preserved in the cores. Macroscopic charcoal samples and terrestrial leaf material in the sediment cores were identified in-situ and removed with forceps, then transferred into glass vials with deionized water and shipped to the Lawrence Livermore National Laboratory for $^{14}C/^{13}C/^{12}C$ analysis (Table 1). The age model for Lake

Yalahau was created with two radiocarbon dates, performed on detrital charcoal by the Beta Analytic Testing Laboratory (Table S1), and eight previously determined radiocarbon-based age-depth pairs from sediment cores collected in 2017 (core PYA17; Table S2). Equivalent depths were correlated between the 2017 and 2023 cores via geochemical stratigraphy (Fig. 3; Table S3). For these geochemical correlations, variability through time in the abundance of Sr was used because the large-amplitude changes in Sr at Lake Yalahau resulted in easily identifiable peaks in both records. The similar variability in Sr between the two cores allowed us to determine which depths in the 2023 core were equivalent to depths in the 2017 core (Fig. 3). Age models were created using the R package BCHRON (Haslett and Parnell, 2008), which calibrated the radiocarbon ages using the IntCal20 calibration curve (Reimer et al., 2020).

Table 1: Age-depth relationships used to construct the Laguna Maravillas age model.

Depth	Uncalibrated yr BP	Calibrated yr BP	Error	Material Dated	Calibration
Surface	-72	N/A	0	N/A	N/A
41	170	182	30	Charcoal	IntCal20
71.5	235	290.5	35	Charcoal	IntCal20
141.5	3015	3188	35	Charcoal	IntCal20
180	3830	4230.5	35	Charcoal	IntCal20
316	5060	5814	35	Charcoal	IntCal20
349	6530	7464	35	Charcoal	IntCal20
412	6605	7474	35	Charcoal	IntCal20
462	7290	8097.5	40	Leaf	IntCal20

Fig 3. A. A lithological comparison between composite sediment cores recovered from Lake Yalahau in 2023 (Yal23; Table S1) and 2017 (PYA17; Table S2). Calibrated radiocarbon dates obtained from the 2017 core are represented by red squares, while two new radiocarbon dates obtained from the 2023 core are represented by blue circles. Geochronological tie points were correlated via geochemical stratigraphy (black dotted lines). Panels **B.** and **C.** show time series of

variability in bulk Sr through time in the 2017 and 2023 cores, respectively, with red dotted lines showing the tie points used to create the age model used in this study.

3.3 Geochemistry

X-ray fluorescence (XRF) spectroscopy was performed using an Itrax XRF core scanner at the University of Minnesota-Duluth Large Lakes Observatory (Laguna Maravillas) and the Oregon State University Marine and Geology Repository (Lake Yalahau) to measure the elemental compositions of the sediment cores. Elemental abundances – measured in counts per second (cps) of element-specific fluorescent X-ray energies – were recorded at a 0.3 (Lake Yalahau) and 0.5 cm (Laguna Maravillas) resolution, using a Cr source tube at 30 kV and 55 mA, with a 15-second dwell time. Raw elemental concentration data were reprocessed to optimize peak fitting using QSpec 8.6.0 software. To account for potential bias introduced by asymmetry in the raw data, elemental ratio values were log-transformed prior to analyses.

3.4 Loss on ignition

Total organic matter (TOM) and total carbonate material (TC) were calculated for both cores by measuring mass loss during iterative sediment combustion. For each core, approximately 1 cm^3 of sediment was subsampled at a 10 cm resolution, oven-dried overnight at 60˚ C, then combusted in a muffle furnace at 550˚ C for 4 hours and 1000˚ C for two hours. The subsamples were weighed between each of the above steps and the mass differences were recorded. The mass lost during combustion at 550˚ C represented the amount of TOM, while the mass lost during combustion at 1000˚ C represented the amount of TC (Dean, 1974; Heiri et al., 2001).

3.5 Statistical analysis

Principal component analysis (PCA) of the XRF geochemical data was performed to reduce the dimensionality of the dataset and characterize relationships between concentrations of individual elements (Jollife, 1986). The PCA was based on standardized elemental abundances to homogenize the dimensions of the dataset, thus taking the units of all elements to standard deviations. The first two statistically significant principal components (PC1 and PC2) were used to explore correlations among elemental abundances because they are orthogonal, linear combinations of the elements contained in the original dataset (Jolliffe, 1986). Thus, in the plane defined by PC1 and PC2, angles between vectors associated with each element represent correlations among them. Whereas acute and obtuse angles represent positive and negative correlations, respectively, near-right angles indicate independence.

4. Results

4.1 Geochronology and core lithology

The 509 cm Maravillas sediment core spans from 8.7 ka to the present (Fig. 4 A). The deepest stratigraphic unit of the core, spanning 509 to 480 cm, represents the period between 8.7 and 8.4 ka. This unit is characterized by very dense, mottled brown and gray clay. Between 480 and 340 cm (8.46 to 6.38 ka), the sediments transition to a homogeneous and massive unit composed primarily of brown silt and clay. Organic matter content increases above this depth, resulting in a stratigraphic unit characterized by dark brown clay containing macroscopic woody plant debris and detrital charcoal between 340 and 240 cm (6.4 to 4.5 ka). The unit spanning 240 to 120 cm (4.5 to 2.3 ka) is composed of black silt and clay and abundant aquatic plant material. Between 120 and 48 cm (2.3 to 0.3 ka), the sediments are characterized by mottled gray and tan silt and fine sand, with abundant intact gastropod shells near the top of the unit. The uppermost 48 cm – spanning 0.8 ka to the present – is composed of black silt and clay and contains oxidized Fe-rich nodules throughout.

The 540 cm Yalahau sediment core spans from 8.4 ka to the present (Fig. 4 B). The deepest stratigraphic unit of the core, from 540 to 468 cm, spans from 8.4 to 6.5 ka and is composed of dark brown, peaty sediment intercalated with macroscopic woody debris and plant material. Between 468 and 187 cm (6.4 to 1.1 ka), the sediments are characterized by laminae made up of alternating dark and light clay. Above 187 cm (1.1 ka), the sediments transition to a homogeneous and massive unit composed primarily of brown silt and clay that persists until 12 cm (-10 years before present). Between 12 cm and the sediment-water interface – sediments deposited during the past few decades – the sediments are homogenous and water-saturated.

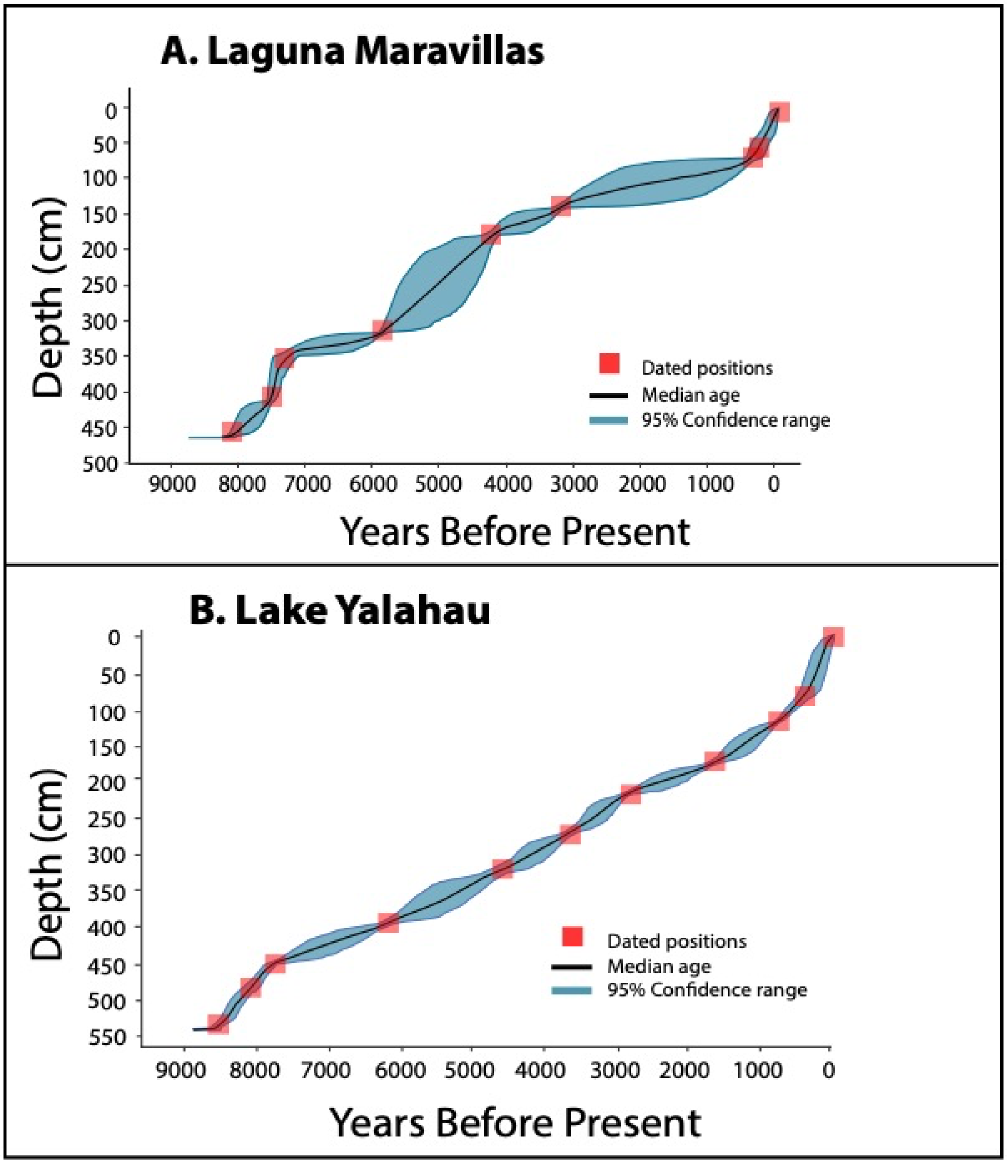

Fig. 4. Age models for **A.** Laguna Maravillas and **B.** Lake Yalahau. The median calibrated age-depth relationships, which were used for interpolating and plotting the data used in this study, are represented by the black line. The 95% confidence interval for these age-depth relationships is shaded in blue.

4.2 XRF geochemistry

For this study, we focused on element concentrations that have been previously demonstrated to be indicators of precipitation at other Mesoamerican sites (e.g., Duarte et al., 2021) and ratios between terrigenous and authigenic elements, which have been shown to indicate the degree of local evaporation (e.g., Gibson et al., 2024) (Fig. S1). At Laguna Maravillas, the first principal component (PC1) explains 67% of the variance in the XRF dataset. Elements commonly associated with terrestrial sources (e.g., Fe, Ti, K, and Zr) are positively correlated with PC1 (Fig. 5 A) and PC1 scores are generally antiphased with the ratio of Ca to Zr (Ca/Zr) (Fig. 6, A and B). Between 8.3 ka and 5.1 ka, PC1 scores gradually decrease, while Ca/Zr increases. Between 5.1 ka and 3.8 ka, both proxies show increased variability, with low PC1 scores (high Ca/Zr) between 5.1 ka-4.8 ka, high PC1 scores (low Ca/Zr) between 4.8 ka-4.6 ka, and low PC1 scores (high Ca/Zr) between 4.3 ka-3.8 ka. During the interval spanning 4.3 ka to 3.8 ka, PC1 scores reach the lowest values of the entire record (-3.4 at 3.8 ka), while Ca/Zr values are higher than during any other interval. During the transition into the Late Holocene, PC1 scores initially increase, then gradually decrease while remaining moderately high, until ca. 1.5 ka. The Ca/Zr values show generally opposite trends during this interval, with a decrease between 3.7 ka and 2.3 ka and subsequent increase between 2.3 ka and 1.5 ka. A hiatus in sedimentation occurred between 1.5 ka and 0.84 ka, after which point both variables remain antiphased, but are highly variable and show large amplitude, centennial-scale fluctuations.

At Lake Yalahau, PC1 explains 38.6% of the data variance and is most strongly correlated with Si and elements associated with authigenic minerals (e.g., Ca, Sr) (Fig. 5 C). Lake Yalahau PC1 scores increase through the Middle Holocene, with PC1 reaching its highest score (4.4) at 6.1 ka and remaining high until 4.8 ka (Fig. 5 C). Between 4.8 and 4.4 ka, PC1 scores decrease, then, at 4.3 ka, PC1 scores increase and reach a local maximum of 1.8, before decreasing again until 4.1 ka. After 4.1 ka, PC1 scores gradually increase to 2.9 at 2.7 ka. After 2.7 ka, PC1 scores decrease through the present. The Ca/Zr at Lake Yalahau show an increasing trend between 8.0 ka and 6.5 ka and decreasing values between 6.5 ka and 5.0 ka. Between 5.0 and 4.1 ka, Ca/Zr values are high and reach a local maximum at 4.28 ka. After 4.1 ka, Ca/Zr values gradually decrease to the present (Fig. 6 H).

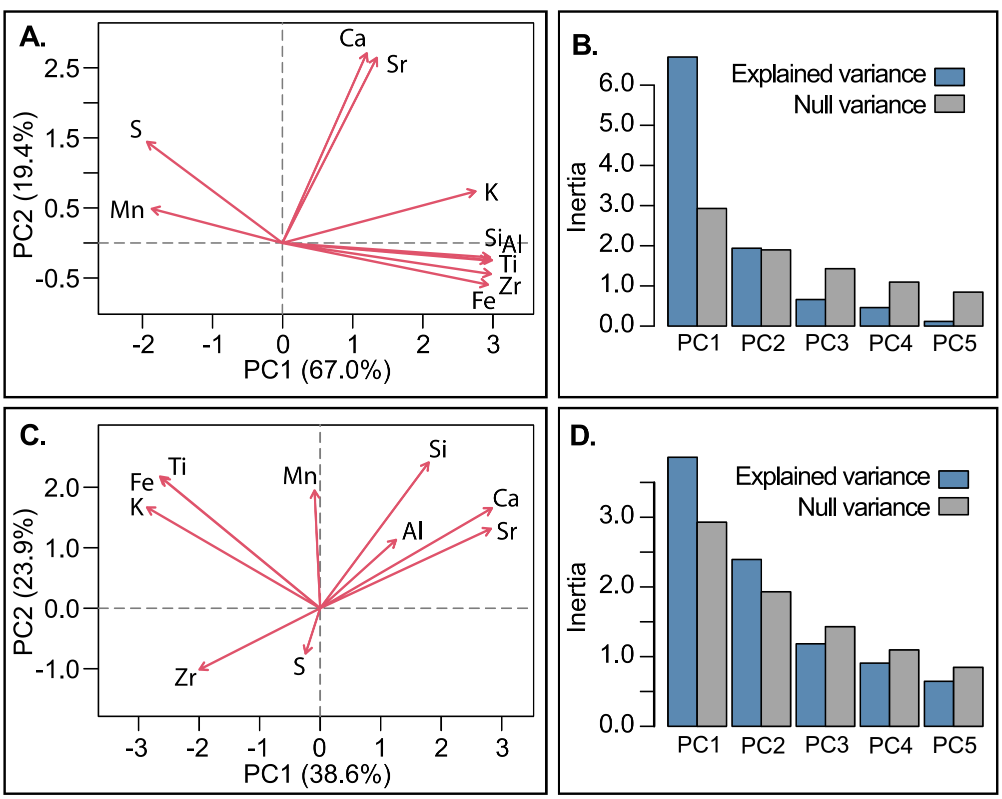

Fig. 5. PCA biplots of the XRF geochemical data from **A.** Laguna Maravillas and **C.** Lake Yalahau. At Laguna Maravillas, elements associated with clastic minerals delivered via catchment weathering and erosion are positively correlated with PC1, while PC2 is positively

correlated with elements associated with authigenic lake production. At Lake Yalahau, PC1 is positively correlated with elements associated with authigenic minerals and negatively correlated with clastic minerals. PC2 values at Lake Yalahau are most strongly influenced by variability of manganese (Mn) and sulfur (S), and thus likely reflects redox conditions through time. Statistical significance for each of the principal components was tested using the broken stick method, whereby the PCA results from **B.** Laguna Maravillas and **D.** Lake Yalahau were considered to be significant if the amount of variance explained by a principal component was greater than the variance explained by random variability.

4.3 % TOM and % TC

Loss on ignition results showed variability through time in the relative amounts of TOM and TC for both cores. In the Laguna Maravillas sediments, % TOM is generally high between 8.5 and 6.5 ka, with an average of 83.5%. After 6.5 ka, % TOM gradually decreases to a local minimum of 21.4% at 4.5 ka. Between 4.4 and 4.2 ka, % TOM increases and peaks at 46.1% at 4250 years before present. After this interval, % TOM decreases again and remains low (with an average of 26.5%) until 3.1 ka. Between 3.1 and 0.4 ka, % TOM averages 74.3 %, then decreases to an average of 48.3% during the last 300 years (Fig 6 B). Percent TC is generally low and showes little variability between 8.5 and 4.5 ka. During this interval, % TC ranges from 1.5 to 4.5%. Between 4.4 and 4.2 ka, % TC increases to a local maximum of 7.9%, then decreases to 1.9% at 3.5 ka. Percent TC then gradually increases to 15.8% at 0.4 ka, before decreasing to an average of 3.1% during the last 300 years (Fig. 6 C).

At Lake Yalahau, % TOM is generally high and shows little variability between 7.6 and 3.2 ka, with an average of 64.3%. Percent TOM gradually decreases between 3.2 and 1.9 ka, where it reaches the lowest value of the entire record (18.9%). Percent TOM then increases to 50.5% at 1.4 ka and averages 52.1% between 1.4 ka and the present (Fig. 6 F). Percent TC at Lake Yalahau is generally in phase with % TOM, with high values during the Middle Holocene and gradually decreasing values during the Late Holocene. Percent TC reaches their highest values between 4.9 and 4.2 ka, before decreasing through the present (Fig. 6 G).

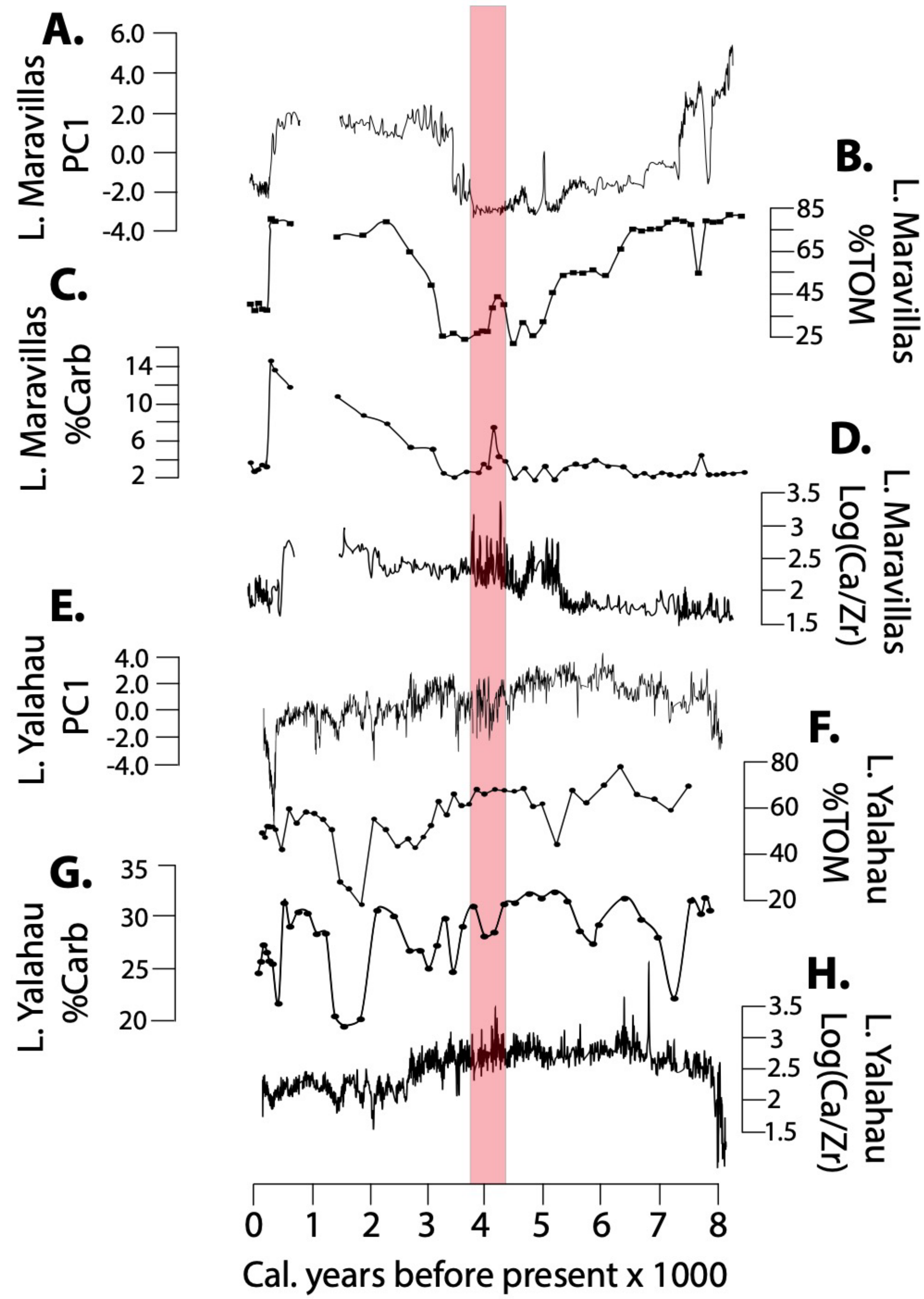

Fig. 6. Time series of geochemical and loss on ignition data from the Laguna Maravillas and Lake Yalahau sediment cores. **(A and E)** Time series of PC1 scores at Laguna Maravillas and Lake Yalahau represent variability through time in the aggregated flux of elements associated with detrital and authigenic minerals, respectively. **(B and F)** Variability through time in the

relative amount of total organic matter (% TOM) in the Laguna Maravillas and Lake Yalahau sediments. Changes in % TOM were interpretated to represent lake level variability such that high % TOM values represent low lake levels and vice versa. **(C and G)** Variability through time in the relative amount of total carbonate material (% TC) in the Laguna Maravillas and Lake Yalahau sediments. During dry intervals, increased evaporation would intensify authigenic carbonate production, leading to increased % TC values. **(D and H)** The ratio of Ca to Zr reflects the intensity of carbonate saturation and authigenic calcite precipitation, relative to the amount of terrigenous material transported to the lake basin via precipitation and runoff. When precipitation was reduced and/or aridity was high, Ca/Zr values increased. When aridity was low, Ca/Zr decreased.

5. Discussion

5.1 Geochemical proxies of precipitation and evaporation in the Yucatán Peninsula

Geochemical analysis using XRF data from sediment cores has been demonstrated to be an effective way to reconstruct past climatic and environmental changes (e.g., Duarte et al., 2021). However, it is often difficult to interpret local scale changes in the ratio of precipitation to evaporation (P/E) from the flux of any individual element because many factors can influence element delivery and cycling in a lacustrine system (Mark et al., 2022). For example, terrestrially sourced elements are commonly interpreted to reflect watershed-scale precipitation-driven runoff (e.g., Haug et al., 2001). However, XRF measurements of terrigenous elements in sediment cores – such as Ti, Zr, and Fe – can also be influenced by the average grain size distribution and specific gravity of the sediments themselves (Brown, 2015). Similarly, Si can be interpreted to represent terrestrial siliceous mineral transport and deposition but is also associated with biogenic silica production by diatom communities in the water column (Peinerud, 2000). Evaporation proxies can also suffer from interpretative ambiguity, especially in carbonate-rich regions, because increases in elements commonly associated with authigenic sources, such as Ca, can be interpreted as reflecting either a decrease in lake volume (drier conditions) or an increase in terrestrially sourced carbonate runoff (wetter conditions) (Lu et al., 2017). To mitigate potential uncertainty associated with the flux of any single element, we focused our interpretations on the aggregated total flux of elements represented by the first principal components in our PCA analyses and on ratios of elements that were shown by our PCA results to have opposite drivers (e.g., Ca and Zr).

In both records, the contrast between lithogenic and authigenic elements define the first principal component (Fig. 5), implying that the main mode of variability through time at both sites was probably associated with precipitation changes. Terrestrially sourced elements define PC1 of the Laguna Maravillas record (Fig. 5 A), with positive PC1 scores representing high watershed erosion and transport (i.e., wetter conditions) and negative scores representing periods when they were low (drier conditions). In the Lake Yalahau record, the negative scores of PC1 were defined by terrestrial material, whereas the positive end was defined by Si and elements associated with authigenic carbonate production (Fig. 5 C), so periods characterized by high PC1 scores at Lake Yalahau represent either increased carbonate precipitation under dry conditions, increased biogenic silica production by diatom communities, or increased watershed transport of silicious minerals. The latter of those scenarios is unlikely, since the other terrigenous elements were negatively correlated with PC1. Nevertheless, the addition of Si to the authigenic elements in the aggregate Lake Yalahau PC1 resulted in PC1 scores that only reflected 38.6% of the dataset variance and a time series that did not strongly correlate with the other P/E indicators from that site.

The Ca/Zr ratio from both records provides additional insight into local scale hydrology. The ratio of authigenic to terrigenous elements in sediment cores from karstic lakes has been shown to respond to changes in aridity such that periods of increased evaporation increase water column carbonate saturation and deposition (i.e., increase solid Ca and Sr precipitation) (Van der Meeren et al., 2022). Arid conditions likewise reduce the rate of erosion and transport of terrigenous elements into the lake (i.e., decrease Ti, Zr, and Fe deposition) (Duarte et al., 2021). We chose Zr as our terrigenous end member because our XRF data showed that Zr presented the same trends as Ti and Fe, but had lower overall concentrations and higher relative variability. Therefore, when plotted as a ratio, the Ca/Zr data were able to best show evaporation trends through time – epecially during dry intervals – because the terrestrial end member (Zr) was not entering the system at such a constantly high rate as Ti or Fe (Fig. S1). Changes in Ca/Zr through time thus reflect local scale P/E variability, with dry intervals associated with elevated Ca/Zr and vice versa.

Supporting our geochemical data, the variability in % TOM and % TC in the Laguna Maravillas and Lake Yalahau sediments provide independent proxies for lake level changes and local scale precipitation/evaporation (e.g., Dean, 1974; Shuman et al., 2001; Zhang et al., 2003). While % TC is generally reflective of local changes in aridity, driven by authigenic carbonate precipitation during evaporation (Zhang et al., 2003), many factors can influence % TOM in sediments. In our cores, we interpret changes in % TOM to primarily reflect changes in lake level through time. Due to the dense vegetation in the watersheds and littoral zones at Laguna Maravillas and Lake Yalahau, reductions in lake level would bring organic matter closer to the coring sites, thereby increasing % TOM in the sediments deposited during those intervals. This interpretation is supported in two ways: First, % TOM and % TC in both cores were generally in phase with each other. When evaporation was high (i.e., high % TC), % TOM was also high and vice versa. Secondly, Laguna Maravillas shows a much greater degree of variability in % TOM, which would be expected due to the hydrologically closed nature of the lake. Without permanent inflows, lake levels at Maravillas are susceptible to large amplitude changes based on the local balance of precipitation to evaporation. Lake Yalahau does not show the same large amplitude shifts in % TOM, likely because its connection to groundwater allows lake levels to remain comparatively stable, even during periods of increased aridity.

5.2 A geochemical expression of the 4.2 ka event in the western hemisphere tropics

Our geochemical analyses indicate that P/E in the central and northern Mexican Yucatán Peninsula progressively decreased between 8 and 5 ka (Fig. 6; Fig 7, A and B). These interpretations are consistent with other paleoclimatic reconstructions from the northern Yucatán Peninsula, which also show comparatively drier conditions during the early and Middle Holocene than during the Late Holocene (Carillo-Bastos et al., 2010). However, this contrasts with records developed from the southern Yucatán peninsula, which show that P/E in Guatemala progressively increased through the early and Middle Holocene (Winter et al., 2020; Duarte et al., 2021; Obrist-Farner et al., 2022). These poorly correlated Yucatán rainfall trends during the Early and Middle Holocene are in line with modern and Late Holocene analyses of regional precipitation, which have previously demonstrated differential precipitation responses between the northern and southern Yucatán regions (Medina-Elizalde, et al., 2010; Douglas et al., 2015).

Despite precipitation differences during the Early and Middle Holocene, a regionally coherent hydroclimate signal emerged in the Yucatán Peninsula during the transition between the Middle and Late Holocene (Fig. 6; Fig. 7, A-C; Fig. 8, A-E). Comparisons between our geochemical data from Mexico and hydroclimate proxy records from sediment cores (Stansell et al., 2020; Duarte et al., 2021) and speleothems (Winter et al., 2020) from Guatemala show that precipitation across the region was punctuated by centennial scale dry conditions between 4.3 and 4.0 ka (Fig. 8, A-E). The timing of this dry interval in the Yucatán is similar to proxy records of drought from North America (Booth et al., 2005), South America (Ohlendorf et al., 2014), Europe (Zanchetta et al., 2016; Psomiadis et al., 2018), and Asia (Staubwasser et al, 2003; Zhang et al., 2018), supporting the hypothesis that the drying recorded in our cores are local expressions of global-scale drying that occurred during the end of the Middle Holocene (Fig. 7). After this dry interval and through the Late Holocene, the regional coherency of hydroclimate records became weak once again, suggesting that the widespread aridity that occurred during the 4.2 ka event was unique in its spatial expression and driven by synoptic scale ocean-atmosphere forcings capable of driving widespread hydroclimatic responses.

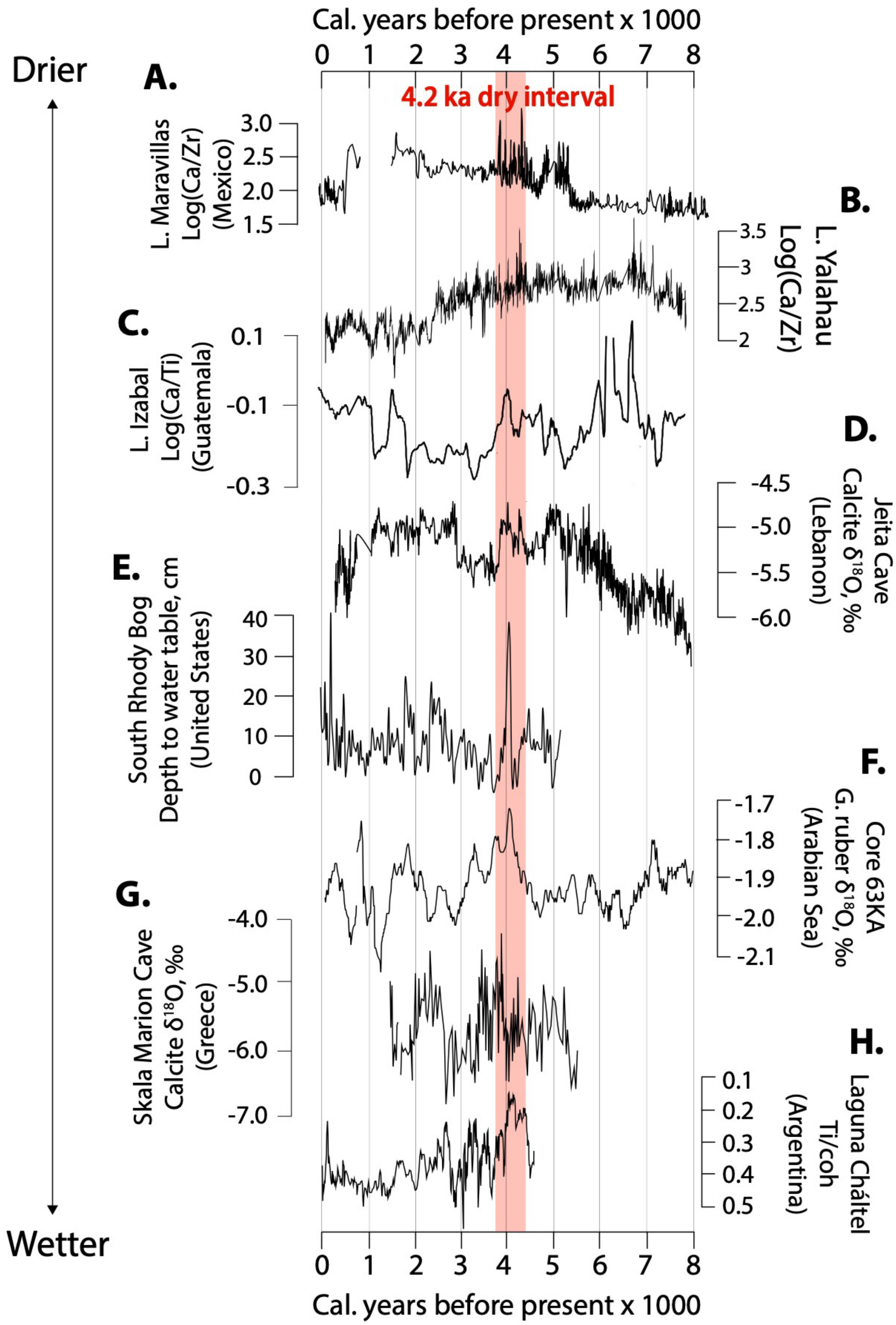

Fig. 7. Indicators of drying during the 4.2 ka event from our new records compared with existing records from selected regions around the world (for a full review of sites impacted during this

event, see Railsback et al., 2018 and Renssen, 2022). **(A-C)** Geochemical indicators of precipitation and evaporation in the Yucatán Peninsula (from this study and Duarte et al. (2021)). **(D)** Speleothem calcite $\delta^{18}O$ from Jeita Cave, Lebanon (Cheng et al., 2015). **(E)** Water table depth fluctuations in the northern United States inferred from testate amoeba assemblages (Booth et al., 2005). **(F)** Precipitation variability in the Arabian Sea region, based on $\delta^{18}O$ preserved in *G. ruber* tests in sediment cores (Staubwasser et al., 2003). **(G)** Precipitation variability reconstructed from speleothem calcite $\delta^{18}O$ in Skala Marion Cave, Greece (Psomiadis et al., 2018). **(H)** Variability in precipitation-driven catchment erosion and runoff at Laguna Chátel, Argentina (Ohlendorf et al., 2014).

5.3 Synoptic origins of the 4.2 ka drying event

The hydroclimate trends observed in our data occurred within the global context of decreasing Northern Hemisphere insolation and mean annual temperature during the Holocene (Laskar et al., 2004). This has been shown to have driven a steady southward migration of the ITCZ between 9 and 4.5 ka (Haug et al., 2001). During the transition between the middle and Late Holocene, Northern Hemisphere insolation and mean annual temperature continued to decrease (Laskar et al., 2004; Zhang et al., 2022) and the rate of southerly displacement of the ITCZ increased (Haug et al., 2001). During this time, decreasing Northern Hemisphere insolation and temperature reduced the SST gradient between the eastern and western Pacific Ocean and consequently weakened easterly Pacific trade winds (Koutavas et al., 2006). The decreased equatorial SST gradient and subdued easterly trade winds during that time reduced upwelling along the western coast of the Americas and ultimately increased the frequency and magnitude of El Niño events during the middle-to-Late Holocene transition (Haug et al., 2001; Conroy et al.,

2008) (Fig 8, H-K). Recent climate model experiments showed that these El Niño-driven SST anomalies may have worked constructively with the desertification of northern Africa and the Middle East during the transition into the Late Holocene to collectively modulate global precipitation patterns (Rensson, 2022). Timing of these combined ocean-atmosphere drivers coincided with geochemical indicators of increased evaporation and decreased catchment erosion across the Yucatán Peninsula (Fig. 6; Fig 8, A-E).

Mechanistically, an increase in El Niño frequency would have impacted precipitation in the Yucatán Peninsula through the relationship between ENSO-driven sea level pressure (SLP) anomalies and the CLLJ. Specifically, El Niño events have been shown to increase SLP over the Caribbean basin during the summer (Wang, 2007). In turn, high Caribbean SLP would induce a westward expansion of the North Atlantic Subtropical High pressure system (NASH), strengthening the CLLJ and diverting it to the south (Gibson et al., 2024). Through this ENSO-NASH-CLLJ relationship, a strong CLLJ has been shown to produce negative rainfall anomalies across the circum-Caribbean region (Cook and Vizy, 2010). Our data therefore suggest that increased El Niño activity, driven by reduced equatorial Pacific SST gradients related to a southerly displaced ITCZ, played a role in the dry conditions associated with the 4.2 ka dry interval by increasing Caribbean SLP. This likely resulted in a westward expansion of the NASH, a strengthened and southerly CLLJ, and an overall reduction in precipitation in the Yucatán Peninsula.

After the transition to the Late Holocene, the regional coherency of hydroclimate records in western Central America weakened (Fig 8, A-E), suggesting that additional synoptic hydroclimatic drivers began to exert controls on precipitation. For example, around 2.5 ka, lake sediment cores collected from southwestern Greenland showed an increase in hypolimnetic anoxia that persisted through the present (Olsen et al., 2012). These data have been used to infer that a mean-state shift to persistently +NAO conditions occurred during, and persisted through, the Late Holocene. These conditions may have increased the influence of the NASH, which has been shown to impact precipitation delivery to western Central America in both the modern instrumental and paleoclimatic records (Bhattacharya et al., 2017; Gibson et al., 2024). However, ENSO and the NAO do not homogeneously affect Central American precipitation and can interfere with one another, either positively or negatively (Giannini et al., 2001; Bhattacharya et al., 2017). It is therefore possible that strengthening +NAO conditions during the Late Holocene increased aridity at some sites in the Yucatán and western Central America more strongly than at others. Nevertheless, the agreement of drying signals observed across Central America during the Middle-to-Late Holocene transition, and the regional incoherency before and after that time, suggest that the anomalous drying that occurred during the 4.2 ka event was due to a unique combination of forces capable of causing widespread aridity across a region that is otherwise notably heterogeneous in its expression of hydroclimatic conditions (Steinman et al., 2022; Obrist-Farner et al., 2023). Specifically, the comparisons between our data and records of global ocean-atmosphere variability indicate that an increase in the frequency of El Niño events during the transition into the Late Holocene coincided with records of aridity across the Yucatán Peninsula and western Central America, suggesting that changing ENSO dynamics played a leading role in the widespread drying associated with the 4.2 ka event.

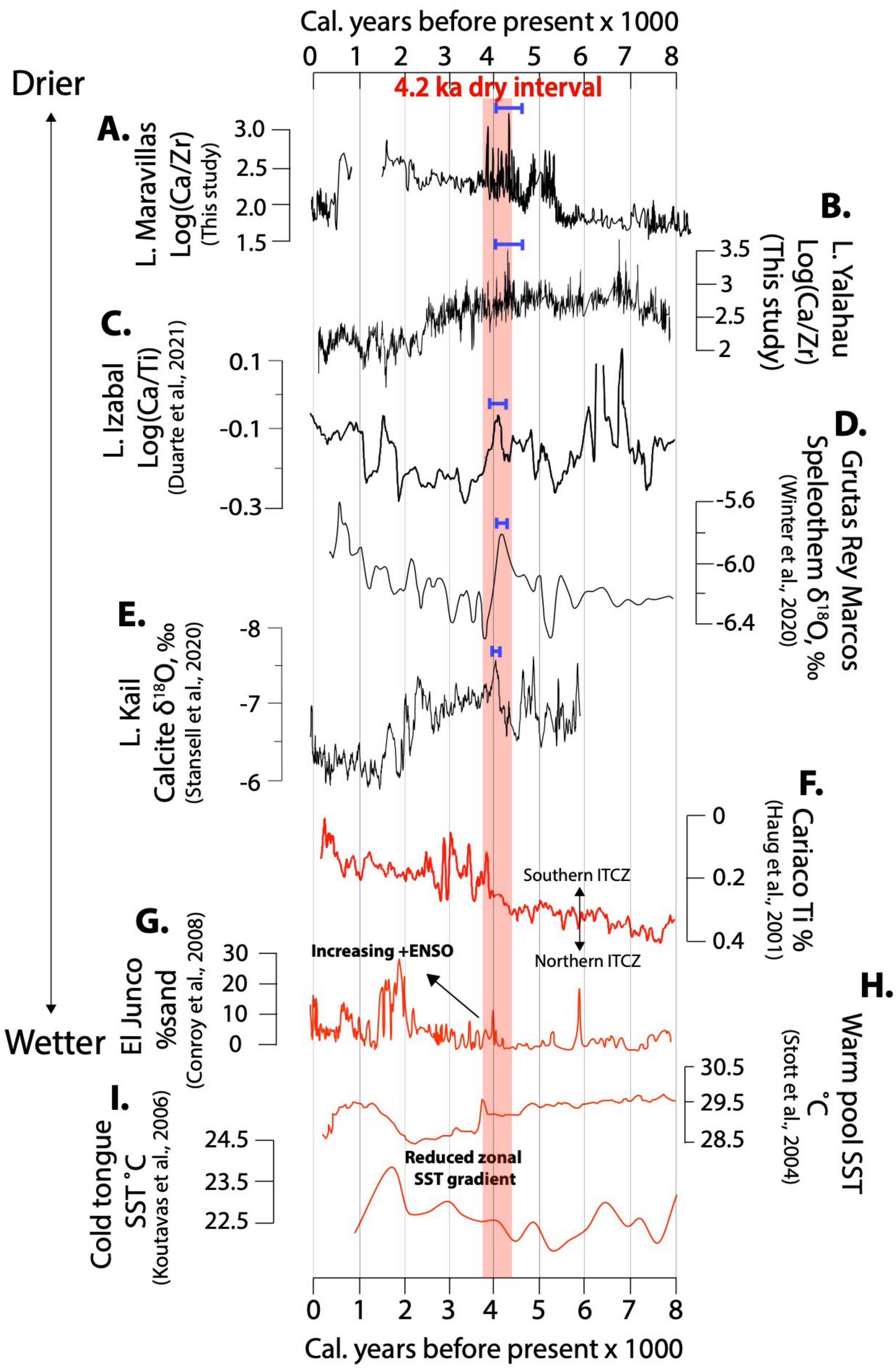

Cal. years before present x 1000
0 1 2 3 4 5 6 7 8
4.2 ka dry interval
Drier
Wetter
A.
L. Maravillas Log(Ca/Zr)
(This study)
3.0 2.5 2.0 1.5
B.
L. Yalahau Log(Ca/Zr)
(This study)
3.5 3 2.5 2
C.
L. Izabal Log(Ca/Ti)
(Duarte et al., 2021)
0.1 -0.1 -0.3
D.
Grutas Rey Marcos Speleothem δ18O, ‰
(Winter et al., 2020)
-5.6 -6.0 -6.4
E.
L. Kail Calcite δ18O, ‰
(Stansell et al., 2020)
-8 -7 -6
F.
Cariaco Ti %
(Haug et al., 2001)
0 0.2 0.4
Southern ITCZ
Northern ITCZ
G.
El Junco %sand
(Conroy et al., 2008)
30 20 10 0
Increasing +ENSO
H.
Warm pool SST °C
(Stott et al., 2004)
30.5 29.5 28.5
I.
Cold tongue SST °C
(Koutavas et al., 2006)
24.5 23.5 22.5
Reduced zonal SST gradient

Fig. 8. Hydroclimate proxies (black lines) and synoptic climate records (red lines). **(A and B)** Geochemical indicators of precipitation and evaporation from the Mexican Yucatán Peninsula. **(C)** Geochemical indicators of precipitation and evaporation from Lake Izabal, located on the Caribbean coast of Guatemala. **(D)** Speleothem oxygen isotope ratios from Grutas Rey Marcos, central Guatemala. **(E)** Bulk sediment carbonate $\delta^{18}O$ from Lake Kail, western Guatemala. **(F)** Ti flux into the Cariaco Basin, which has been interpreted as a function of fluvial discharge variability associated with migrations of the ITCZ. **(G)** The El Junco Holocene ENSO record, which shows an increase in the frequency of +ENSO events beginning ca. 4.2 ka. **(H and I)** Records of the Pacific warm pool and cold tongue SST variability and changes in the SST gradient between the eastern and western Pacific during the past 8 ka. Blue brackets above the hydroclimate proxies show the 95% confidence band for the timing of peak aridity during the 4.2 ka event.

6. Conclusions

Geochemical indicators of local-scale hydrologic variability in the Yucatán Peninsula provide evidence for an expression of the 4.2 ka drying event in the northern Neotropics. This event has previously been identified in many climate records from the Eastern and Western hemispheres. However, records of the 4.2. ka event in northern tropical America are exceedingly rare, making it difficult to ascertain the synoptic drivers and full spatial extent of dry conditions during this interval. Our data indicate that the 4.2 ka event caused drier conditions in the Yucatán Peninsula, likely driven by a combination of oceanic and atmospheric processes controlling precipitation in the region. Specifically, the dry interval coincided with a mean-state reduction in zonal SST gradients in the Pacific Ocean, which increased ENSO variability and the frequency of El Niño events. After the 4.2 ka event, and through the Late Holocene, the regional coherency of hydroclimate records in the Yucatán region weakened, suggesting that additional synoptic climatic drivers began to influence local-scale hydrology. The good agreement between Yucatán proxy records during the 4.2 ka event, and their generally weak correlation before and after that period, suggests that climatic forces during the transition between the Middle and Late Holocene were unique in their ability to drive regionally coherent hydrologic changes across western Central America. When compared with existing records of Holocene ENSO variability, our data suggests that stronger and more frequent El Niño events may have played a role in forcing global scale drying during the Middle-to-Late Holocene transition.

7. Supplementary Information

Supplementary Table S1: Age depth relationships and radiocarbon metadata for the new Lake Yalahau cores recovered in 2023, determined via radiocarbon accelerated mass spectroscopy of detrital carbon sources.

Depth (cm)	Uncalibrated yr BP	Error	Frac. modern	Calibrated yr BP	Calibration
411.5	7190	47	40.86	7990	IntCal20
459.5	7600	36	38.82	8400	IntCal20

Table S2: Same as table S1, but for the Lake Yalahau cores recovered in 2017 core (core PYA17).

Depth (cm)	Uncalibrated yr BP	Error	Frac. Modern	Calibrated yr BP	Calibration
Surface	-73	0	N/A	N/A	N/A
50	365	36	0.9556	459	IntCal20
82	781	30	0.9074	701	IntCal20
149	1697	29	0.8096	1578	IntCal20
219	2703	36	0.7143	2809	IntCal20
286	3334	26	0.6603	3537	IntCal20
337	4064	28	0.603	4562.5	IntCal20
421	5300	28	0.517	6060	IntCal20
503	6843	32	0.4266	7677.5	IntCal20

Table S3: The combined age model table for Yal23, consisting of the newly obtained radiocarbon dates from Table S1 and the depth-corrected radiocarbon dates from Table S2.

Depth	Uncalibrated yr BP	Error	Frac. Modern	Calibrated yr BP	Calibration
0	-73	0	N/A	N/A	N/A
92	365	36	0.9556	459	IntCal20
120	781	30	0.9074	701	IntCal20
177	1697	29	0.8096	1578	IntCal20
220	2703	36	0.7143	2809	IntCal20
272	3334	26	0.6603	3537	IntCal20
327	4064	28	0.603	4562.5	IntCal20
395	5300	28	0.517	6060	IntCal20
451	6843	32	0.4266	7677.5	IntCal20
490	7190	47	0.4086	7990	IntCal20
537	7600	36	0.3882	8400	IntCal20

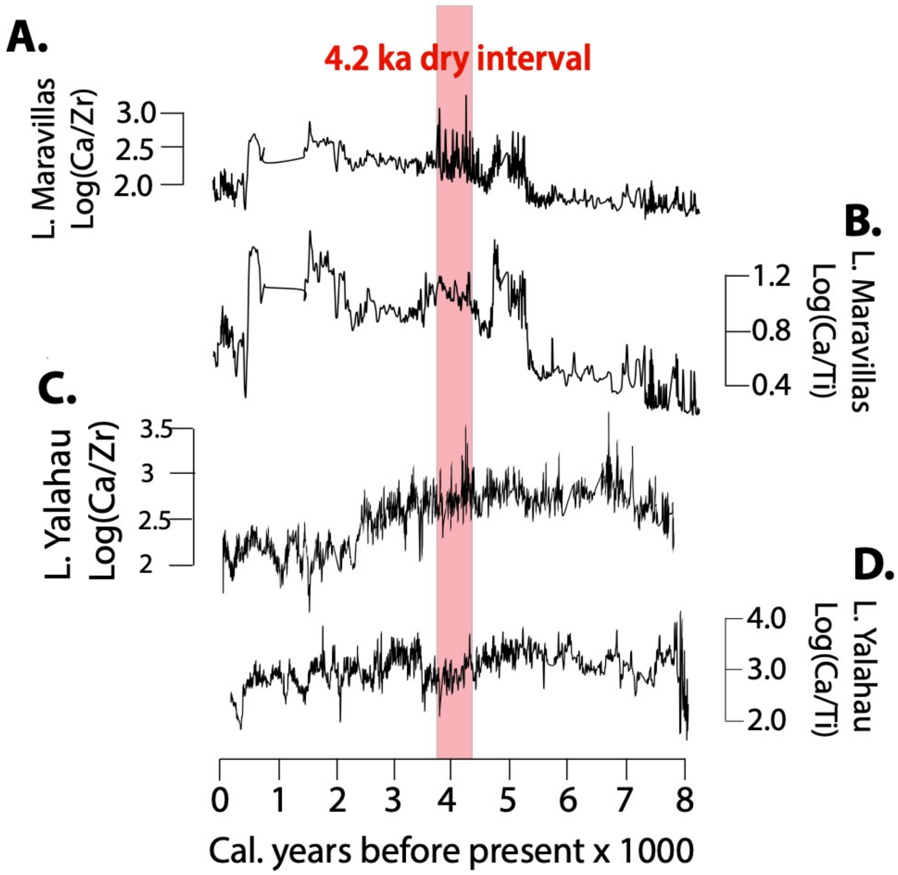

Fig. S1. A comparison between Ca/Zr and Ca/Ti ratios for (**A and B**) Laguna Maravillas and (**C and D**) Lake Yalahau.

8. Funding

This project was supported by funding from the following sources: the U.S. National Science Foundation (award # 2204484) and the Dirección General de Asuntos del Personal Académico, National Autonomous University of Mexico (DGAPA-UNAM; award # IG100722).

9. Author Contributions

Derek Gibson: Conceptualization; Data curation; Formal analysis; Funding acquisition; Writing - original draft; Writing - review & editing. **Jonathan Obrist-Farner:** Writing - review & editing; Methodology; Resources; Software; Supervision. **Alex Correa-Metrio:** Methodology; Resources; Software; Funding acquisition; Data curation; Writing – review & editing. **Alejandra Rodriguez-Abaunza:** Methodology; Data curation; Writing – review & editing. **Carlos Castañeda-Posadas:** Methodology; Investigation; Writing – review & editing

10. Acknowledgements

The authors would like to thank the Continental Scientific Drilling Facility at the University of Minnesota for allowing us to use their laboratory facilities for initial core sampling and storage and the Oregon State University Marine and Geology Repository for performing XRF analysis on the Lake Yalahau sediment cores.

11. Competing interests statement

The authors declare that they have no competing financial or other interests that could affect or have the perception of affecting the author's objectivity or the content of this manuscript.

12. Data availability

Data used for this study are available in the Mendeley data repository: Gibson, Derek (2024), "Laguna Maravillas and Lake Yalahau XRF geochemistry data", Mendeley Data, V3, doi: 10.17632/vp5yk9y2n4.3

13. References

Amador, J.A., Alfaro, E.J., Lizano, O.G. and Magaña, V.O., 2006. Atmospheric forcing of the eastern tropical Pacific: A review. Progress in Oceanography, 69(2-4), pp.101-142.

Anderson, T.G., Anchukaitis, K.J., Pons, D. and Taylor, M., 2019. Multiscale trends and precipitation extremes in the Central American Midsummer Drought. Environmental Research Letters, 14(12), p.124016.

Arz, H.W., Lamy, F. and Pätzold, J., 2006. A pronounced dry event recorded around 4.2 ka in brine sediments from the northern Red Sea. Quaternary Research, 66(3), pp.432-441.

Bhattacharya, T., Chiang, J.C. and Cheng, W., 2017. Ocean-atmosphere dynamics linked to 800–1050 CE drying in mesoamerica. Quaternary Science Reviews, 169, pp.263-277.

Bini, M., Zanchetta, G., Perşoiu, A., Cartier, R., Català, A., Cacho, I., Dean, J.R., Di Rita, F., Drysdale, R.N., Finnè, M. and Isola, I., 2019. The 4.2 ka BP Event in the Mediterranean region: an overview. Climate of the Past, 15(2), pp.555-577.

Blaauw, M. and Christen, J.A., 2011. Flexible paleoclimate age-depth models using an autoregressive gamma process.

Booth, R.K., Jackson, S.T., Forman, S.L., Kutzbach, J.E., Bettis Iii, E.A., Kreigs, J. and Wright, D.K., 2005. A severe centennial-scale drought in midcontinental North America 4200 years ago and apparent global linkages. The Holocene, 15(3), pp.321-328.

Brown, E.T., 2015. Estimation of biogenic silica concentrations using scanning XRF: insights from studies of Lake Malawi sediments. Micro-XRF Studies of Sediment Cores: Applications of a non-destructive tool for the environmental sciences, pp.267-277.

Carrillo-Bastos, A., Islebe, G.A., Torrescano-Valle, N. and González, N.E., 2010. Holocene vegetation and climate history of central Quintana Roo, Yucatán Península, Mexico. Review of Palaeobotany and Palynology, 160(3-4), pp.189-196.

Cheng, H., Sinha, A., Verheyden, S., Nader, F.H., Li, X.L., Zhang, P.Z., Yin, J.J., Yi, L., Peng, Y.B., Rao, Z.G. and Ning, Y.F., 2015. The climate variability in northern Levant over the past 20,000 years. Geophysical Research Letters, 42(20), pp.8641-8650.

Clement, A.C., Seager, R. and Cane, M.A., 2000. Suppression of El Niño during the mid-Holocene by changes in the Earth's orbit. Paleoceanography, 15(6), pp.731-737.

Colinvaux, P. A., P. E. De Oliveira, and J. E. Moreno. 1999. Amazon pollen manual and atlas. Harwood Academic Press., New York.

Conroy, J.L., Overpeck, J.T., Cole, J.E., Shanahan, T.M. and Steinitz-Kannan, M., 2008. Holocene changes in eastern tropical Pacific climate inferred from a Galápagos lake sediment record. Quaternary Science Reviews, 27(11-12), pp.1166-1180.

Cook, K.H. and Vizy, E.K., 2010. Hydrodynamics of the Caribbean low-level jet and its relationship to precipitation. Journal of Climate, 23(6), pp.1477-1494.

Cullen, H.M., Demenocal, P.B., Hemming, S., Hemming, G., Brown, F.H., Guilderson, T. and Sirocko, F., 2000. Climate change and the collapse of the Akkadian empire: Evidence from the deep sea. Geology, 28(4), pp.379-382.

Curtis, S., 2013. Daily precipitation distributions over the intra-Americas sea and their interannual variability. Atmósfera, 26(2), pp.243-259.

Dean, W.E., 1974. Determination of carbonate and organic matter in calcareous sediments and sedimentary rocks by loss on ignition; comparison with other methods. Journal of Sedimentary Research, 44(1), pp.242-248.

Dearing, J.A., 1997. Sedimentary indicators of lake-level changes in the humid temperate zone: a critical review. Journal of paleolimnology, 18, pp.1-14.

De la Barreda, B., Metcalfe, S.E. and Boyd, D.S., 2020. Precipitation regionalization, anomalies and drought occurrence in the Yucatán Peninsula, Mexico. International Journal of Climatology, 40(10), pp.4541-4555.

Douglas, P.M., Pagani, M., Canuto, M.A., Brenner, M., Hodell, D.A., Eglinton, T.I. and Curtis, J.H., 2015. Drought, agricultural adaptation, and sociopolitical collapse in the Maya Lowlands. Proceedings of the National Academy of Sciences, 112(18), pp.5607-5612.

Drysdale, R., Zanchetta, G., Hellstrom, J., Maas, R., Fallick, A., Pickett, M., Cartwright, I. and Piccini, L., 2006. Late Holocene drought responsible for the collapse of Old World civilizations is recorded in an Italian cave flowstone. Geology, 34(2), pp.101-104.

Duarte, E., Obrist-Farner, J., Correa-Metrio, A. and Steinman, B.A., 2021. A progressively wetter early through Middle Holocene climate in the eastern lowlands of Guatemala. Earth and Planetary Science Letters, 561, p.116807.

Dunning, N.P., Beach, T., Sierra, L.G., Jones, J.G., Lentz, D.L., Luzzadder-Beach, S., Scarborough, V.L. and Smyth, M.P., 2013. A tale of two collapses: environmental variability and cultural disruption in the Maya Lowlands. Diálogo Andino-Revista de Historia, Geografía y Cultura Andina, (41), pp.171-183.

Durán-Quesada, A.M., Gimeno, L. and Amador, J., 2017. Role of moisture transport for Central American precipitation. Earth System Dynamics, 8(1), pp.147-161.

Durán-Quesada, A.M., Sorí, R., Ordoñez, P. and Gimeno, L., 2020. Climate perspectives in the intra–Americas seas. Atmosphere, 11(9), p.959.

Giannini, A., Chiang, J.C., Cane, M.A., Kushnir, Y. and Seager, R., 2001. The ENSO teleconnection to the tropical Atlantic Ocean: Contributions of the remote and local SSTs to rainfall variability in the tropical Americas. Journal of Climate, 14(24), pp.4530-4544.

Gibson, D.K., Obrist-Farner, J., Birkett, B.A., Curtis, J.H., Berke, M.A., Douglas, P.M., Rice, P.M. and Maurer, J., 2024. The influence of tropical Atlantic sea-surface temperatures and the North Atlantic Subtropical High during the Maya Droughts. The Holocene, p.09596836231211856.

Haslett, J. and Parnell, A., 2008. A simple monotone process with application to radiocarbon-dated depth chronologies. Journal of the Royal Statistical Society Series C: Applied Statistics, 57(4), pp.399-418.

Haug, G.H., Hughen, K.A., Sigman, D.M., Peterson, L.C. and Rohl, U., 2001. Southward migration of the intertropical convergence zone through the Holocene. Science, 293(5533), pp.1304-1308.

Heiri, O., Lotter, A.F. and Lemcke, G., 2001. Loss on ignition as a method for estimating organic and carbonate content in sediments: reproducibility and comparability of results. Journal of paleolimnology, 25, pp.101-110.

Hodell, D.A., Brenner, M., Curtis, J.H., Medina-González, R., Can, E.I.C., Albornaz-Pat, A. and Guilderson, T.P., 2005. Climate change on the Yucatán Peninsula during the little ice age. Quaternary Research, 63(2), pp.109-121.

Jolliffe, I. T. 1986. Principal Component Analysis. Springer-Verlag, Berlin.

Joyce, T.M., Deser, C. and Spall, M.A., 2000. The relation between decadal variability of subtropical mode water and the North Atlantic Oscillation. Journal of Climate, 13(14), pp.2550-2569.

Koutavas, A., Demenocal, P.B., Olive, G.C. and Lynch-Stieglitz, J., 2006. Mid-Holocene El Niño–Southern Oscillation (ENSO) attenuation revealed by individual foraminifera in eastern tropical Pacific sediments. Geology, 34(12), pp.993-996.

Laskar, J., Robutel, P., Joutel, F., Gastineau, M., Correia, A.C. and Levrard, B., 2004. A long-term numerical solution for the insolation quantities of the Earth. Astronomy and Astrophysics, 428(1), pp.261-285.

Li, C.H., Li, Y.X., Zheng, Y.F., Yu, S.Y., Tang, L.Y., Li, B.B. and Cui, Q.Y., 2018. A high-resolution pollen record from East China reveals large climate variability near the Northgrippian-

Meghalayan boundary (around 4200 years ago) exerted societal influence. Palaeogeography, Palaeoclimatology, Palaeoecology, 512, pp.156-165.

Liu, F. and Feng, Z., 2012. A dramatic climatic transition at~ 4000 cal. yr BP and its cultural responses in Chinese cultural domains. The Holocene, 22(10), pp.1181-1197.

Lu, Y., Fritz, S.C., Stone, J.R., Krause, T.R., Whitlock, C., Brown, E.T. and Benes, J.V., 2017. Trends in catchment processes and lake evolution during the late-glacial and early-to mid-Holocene inferred from high-resolution XRF data in the Yellowstone region. Journal of Paleolimnology, 58, pp.551-569.

Magaña, V., Amador, J.A. and Medina, S., 1999. The midsummer drought over Mexico and Central America. Journal of Climate, 12(6), pp.1577-1588.

Marchant, R. and Hooghiemstra, H., 2004. Rapid environmental change in African and South American tropics around 4000 years before present: a review. Earth-Science Reviews, 66(3-4), pp.217-260.

Mark, S.Z., Abbott, M.B., Rodbell, D.T. and Moy, C.M., 2022. XRF analysis of Laguna Pallcacocha sediments yields new insights into Holocene El Niño development. Earth and Planetary Science Letters, 593, p.117657.

Marín-Stillman, L.E., Pachecho-Ávila, J.G., and Méndez-Ramos, R., 2004. Hidrogeología de la Península de Yucatán, in Jiménez, B., and Marín, L., eds., El Agua en México, Vista desde la Academia: México, D.F., Academia Mexicana de Ciencias, p. 159–176.

Martinez, C., Kushnir, Y., Goddard, L. and Ting, M., 2020. Interannual variability of the early and late-rainy seasons in the Caribbean. Climate Dynamics, 55(5), pp.1563-1583.

Medina-Elizalde, M., Burns, S.J., Lea, D.W., Asmerom, Y., von Gunten, L., Polyak, V., Vuille, M. and Karmalkar, A., 2010. High resolution stalagmite climate record from the Yucatán Peninsula spanning the Maya terminal classic period. Earth and Planetary Science Letters, 298(1-2), pp.255-262.

Meller, H., Arz, H. W., Jung, R., Risch, R., (Eds.), 2200 BC - A Climatic Breakdown as a Cause for the Collapse of the Old World?, Landesmuseum fur Vorgeschichte, Halle, Germany (2015)

Menounos, B., Clague, J.J., Osborn, G., Luckman, B.H., Lakeman, T.R. and Minkus, R., 2008. Western Canadian glaciers advance in concert with climate change circa 4.2 ka. Geophysical Research Letters, 35(7).

Milliken, K.T., Anderson, J.B. and Rodriguez, A.B., 2008. A new composite Holocene sea-level curve for the northern Gulf of Mexico. Geological Society of America Special Papers, 443(1), pp.1-11.

Nakamura, A., Yokoyama, Y., Maemoku, H., Yagi, H., Okamura, M., Matsuoka, H., Miyake, N., Osada, T., Adhikari, D.P., Dangol, V. and Ikehara, M., 2016. Weak monsoon event at 4.2 ka recorded in sediment from Lake Rara, Himalayas. Quaternary International, 397, pp.349-359.

Obrist-Farner, J., Steinman, B.A., Stansell, N.D. and Maurer, J., 2023. Incoherency in Central American hydroclimate proxy records spanning the last millennium. Paleoceanography and Paleoclimatology, 38(3), p.e2022PA004445.

Ohlendorf, C., Fey, M., Massaferro, J., Haberzettl, T., Laprida, C., Lücke, A., Maidana, N., Mayr, C., Oehlerich, M., Mercau, J.R. and Wille, M., 2014. Late Holocene hydrology inferred from lacustrine sediments of Laguna Cháltel (southeastern Argentina). Palaeogeography, palaeoclimatology, palaeoecology, 411, pp.229-248.

Olsen, J., Anderson, N.J. and Knudsen, M.F., 2012. Variability of the North Atlantic Oscillation over the past 5,200 years. Nature Geoscience, 5(11), pp.808-812.

Peinerud, E.K., 2000. Interpretation of Si concentrations in lake sediments: three case studies. Environmental Geology, 40, pp.64-72.

Pérez, L., Bugja, R., Lorenschat, J., Brenner, M., Curtis, J., Hoelzmann, P., Islebe, G., Scharf, B. and Schwalb, A., 2011. Aquatic ecosystems of the Yucatán peninsula (Mexico), Belize, and Guatemala. Hydrobiologia, 661, pp.407-433.

Psomiadis, D., Dotsika, E., Albanakis, K., Ghaleb, B. and Hillaire-Marcel, C., 2018. Speleothem record of climatic changes in the northern Aegean region (Greece) from the Bronze Age to the collapse of the Roman Empire. Palaeogeography, Palaeoclimatology, Palaeoecology, 489, pp.272-283.

Railsback, L.B., Liang, F., Brook, G.A., Voarintsoa, N.R.G., Sletten, H.R., Marais, E., Hardt, B., Cheng, H. and Edwards, R.L., 2018. The timing, two-pulsed nature, and variable climatic expression of the 4.2 ka event: A review and new high-resolution stalagmite data from Namibia. Quaternary Science Reviews, 186, pp.78-90.

Reimer, P.J., Austin, W.E., Bard, E., Bayliss, A., Blackwell, P.G., Ramsey, C.B., Butzin, M., Cheng, H., Edwards, R.L., Friedrich, M. and Grootes, P.M., 2020. The IntCal20 Northern Hemisphere radiocarbon age calibration curve (0–55 cal kBP). Radiocarbon, 62(4), pp.725-757.

Renssen, H. (2022). Climate model experiments on the 4.2 ka event: The impact of tropical sea-surface temperature anomalies and desertification. The Holocene, 32(5), 378-389.

Rodriguez-Abaunza, A. and Correa-Metrio, A. (2023). Environmental history of the northern maya lowlands: evidence from a karstic lake. PAGES, 31 (1), 12-13

Rowan, D.J., Kalff, J. and Rasmussen, J.B., 1992. Estimating the mud deposition boundary depth in lakes from wave theory. Canadian Journal of Fisheries and Aquatic Sciences, 49(12), pp.2490-2497.

Sáenz, F., Hidalgo, H.G., Muñoz, Á.G., Alfaro, E.J., Amador, J.A. and Vázquez-Aguirre, J.L., 2023. Atmospheric circulation types controlling rainfall in the Central American Isthmus. International Journal of Climatology, 43(1), pp.197-218.

Servicio Meteorológico Nacional. 2024a. Normales climatológicas, Yucatán, Estación Cuzama. https://smn.conagua.gob.mx/tools/RESOURCES/Normales_Climatologicas/Mensuales/yuc/mes31048.TXT.

Servicio Meteorológico Nacional. 2024b. Normales climatológicas, Campeche, Estación Silvituc. https://smn.conagua.gob.mx/tools/RESOURCES/Normales_Climatologicas/Mensuales/camp/mes04031.TXT

Shankar, U., 2021. Cave 'Krem Mawmluh' of Meghalaya plateau–The base of the 'Meghalayan Age' and '4.2 ka BP Event' in Holocene (Anthropocene). International Journal of Ecology and Environmental Sciences, 47(1), pp.49-59.

Shuman, B., Bravo, J., Kaye, J., Lynch, J.A., Newby, P. and Webb III, T., 2001. Late Quaternary water-level variations and vegetation history at Crooked Pond, southeastern Massachusetts. Quaternary Research, 56(3), pp.401-410.

Stansell, N.D., Steinman, B.A., Lachniet, M.S., Feller, J., Harvey, W., Fernandez, A., Shea, C.J., Price, B., Coenen, J., Boes, M. and Perdziola, S., 2020. A lake sediment stable isotope record of late-middle to Late Holocene hydroclimate variability in the western Guatemala highlands. Earth and Planetary Science Letters, 542, p.116327.

Staubwasser, M., Sirocko, F., Grootes, P.M. and Segl, M., 2003. Climate change at the 4.2 ka BP termination of the Indus valley civilization and Holocene south Asian monsoon variability. Geophysical Research Letters, 30(8).

Steinman, B.A., Stansell, N.D., Mann, M.E., Cooke, C.A., Abbott, M.B., Vuille, M., Bird, B.W., Lachniet, M.S. and Fernandez, A., 2022. Interhemispheric antiphasing of neotropical precipitation during the past millennium. Proceedings of the National Academy of Sciences, 119(17), p.e2120015119.

Stott, L., Cannariato, K., Thunell, R., Haug, G.H., Koutavas, A. and Lund, S., 2004. Decline of surface temperature and salinity in the western tropical Pacific Ocean in the Holocene epoch. Nature, 431(7004), pp.56-59.

Thompson, L.G., Mosley-Thompson, E., Davis, M.E., Henderson, K.A., Brecher, H.H., Zagorodnov, V.S., Mashiotta, T.A., Lin, P.N., Mikhalenko, V.N., Hardy, D.R. and Beer, J., 2002. Kilimanjaro ice core records: evidence of Holocene climate change in tropical Africa. science, 298(5593), pp.589-593.

Torrescano-Valle, N. and Islebe, G.A., 2015. Holocene paleoecology, climate history and human influence in the southwestern Yucatán Peninsula. Review of Palaeobotany and Palynology, 217, pp.1-8.

Toth, L.T. and Aronson, R.B., 2019. The 4.2 ka event, ENSO, and coral reef development. Climate of the Past, 15(1), pp.105-119.

Tudhope, A.W., Chilcott, C.P., McCulloch, M.T., Cook, E.R., Chappell, J., Ellam, R.M., Lea, D.W., Lough, J.M. and Shimmield, G.B., 2001. Variability in the El Niño-Southern Oscillation through a glacial-interglacial cycle. Science, 291(5508), pp.1511-1517.

Van der Meeren, T., Verschuren, D., Sylvestre, F., Nassour, Y.A., Naudts, E.L., Aguilar Ortiz, L.E., Deschamps, P., Tachikawa, K., Bard, E., Schuster, M. and Abderamane, M., 2022. A predominantly tropical influence on Late Holocene hydroclimate variation in the hyperarid central Sahara. Science Advances, 8(14), p.eabk1261.

Walker, M.J., Berkelhammer, M., Björck, S., Cwynar, L.C., Fisher, D.A., Long, A.J., Lowe, J.J., Newnham, R.M., Rasmussen, S.O. and Weiss, H., 2012. Formal subdivision of the Holocene Series/Epoch: a Discussion Paper by a Working Group of INTIMATE (Integration of ice-core, marine and terrestrial records) and the Subcommission on Quaternary Stratigraphy (International Commission on Stratigraphy). Journal of Quaternary Science, 27(7), pp.649-659.

Wang, C., 2007. Variability of the Caribbean low-level jet and its relations to climate. Climate dynamics, 29, pp.411-422.

Wanner, H., Brönnimann, S., Casty, C., Gyalistras, D., Luterbacher, J., Schmutz, C., Stephenson, D.B. and Xoplaki, E., 2001. North Atlantic Oscillation–concepts and studies. Surveys in geophysics, 22, pp.321-381.

Winter, A., Zanchettin, D., Lachniet, M., Vieten, R., Pausata, F.S., Ljungqvist, F.C., Cheng, H., Edwards, R.L., Miller, T., Rubinetti, S. and Rubino, A., 2020. Initiation of a stable convective hydroclimatic regime in Central America circa 9000 years BP. Nature Communications, 11(1), p.716.

Zanchetta, G., Regattieri, E., Isola, I., Drysdale, R.N., Baneschi, I. and Hellstrom, J.C., 2016. The so-called "4.2 event" in the central Mediterranean and its climatic teleconnections. Alpine and Mediterranean quaternary, 29(1), pp.5-17.

Zhang, J., Jin, M., Chen, F., Battarbee, R.W. and Henderson, A.C.G., 2003. High-resolution precipitation variations in the Northeast Tibetan Plateau over the last 800 years documented by sediment cores of Qinghai Lake. Chinese Science Bulletin, 48, pp.1451-1456.

Zhang, H., Cheng, H., Cai, Y., Spötl, C., Kathayat, G., Sinha, A., Edwards, R.L. and Tan, L., 2018. Hydroclimatic variations in southeastern China during the 4.2 ka event reflected by stalagmite records. Climate of the Past, 14(11), pp.1805-1817.

Zhang, W., Wu, H., Cheng, J., Geng, J., Li, Q., Sun, Y., Yu, Y., Lu, H. and Guo, Z., 2022. Holocene seasonal temperature evolution and spatial variability over the Northern Hemisphere landmass. Nature Communications, 13(1), p.5334.